ENDOR studies on the N1 di-nitrogen centre in diamond

1992 J. Phys.: Condens. Matter 4 8119

(http://iopscience.iop.org/0953-8984/4/41/007)

J. Phys.: Condens. Matter 4 (1992) 8119–8130. Printed in the UK

ENDOR studies on the N1 di-nitrogen centre in diamond

A Cox, M E Newton and J M Baker
Oxford Physics, Clarendon Laboratory, Parks Road, Oxford OX1 3PU, UK

Received 29 April 1992

Abstract. New ENDOR measurements on the N1 centre confirm the N–C–N^+ model for the defect. The N^+ is in a substitutional site with approximately tetrahedral symmetry. The N–C fragment of the centre resembles the P1 centre, with slightly larger unpaired electron density on the nitrogen, and a smaller quadrupole interaction.

1. Introduction

A considerable variety of EPR centres have been found whose hyperfine structure indicates that they involve two ^{14}N nuclei (Loubser and van Wyk 1978, Ammerlaan 1990). An even greater variety of atomic models for these centres has been proposed by various authors. Some clarification of this confusion was proposed by Newton and Baker (1991a), as a consequence of a definitive determination of the symmetry of the W7 centre, and its hyperfine and quadrupole interactions, using ENDOR (Newton and Baker 1991b).

In this paper we discuss the application of this type of ENDOR measurement to the N1 centre. The centre is described by the following spin Hamiltonian with $S = \frac{1}{2}$, and $I_1 = I_2 = 1$ for the two inequivalent ^{14}N nuclei:

$$H = g\mu_B \boldsymbol{B}\cdot\boldsymbol{S} + \boldsymbol{S}\cdot\mathbf{A}^{(1)}\cdot\boldsymbol{I}^{(1)} + \boldsymbol{S}\cdot\mathbf{A}^{(2)}\cdot\boldsymbol{I}^{(2)} + \boldsymbol{I}^{(1)}\cdot\mathbf{P}^{(1)}\cdot\boldsymbol{I}^{(1)} + \boldsymbol{I}^{(2)}\cdot\mathbf{P}^{(2)}\cdot\boldsymbol{I}^{(2)} - g_N\mu_N\boldsymbol{B}\cdot(\boldsymbol{I}^{(1)}+\boldsymbol{I}^{(2)}). \quad (1)$$

N1 was first observed by Shcherbacova *et al* (1969), and was remeasured by Loubser and van Wyk (1985): the spin-Hamiltonian parameters determined by both groups of authors are given in table 1. Both groups found axial symmetry about ⟨111⟩ for $\mathbf{A}^{(1)}$, but they disagreed about the symmetry of $\mathbf{A}^{(2)}$. The latter is almost isotropic, and it is not clear to us how either group of authors was able to determine the anisotropy, as any multiplicity of lines resulting from it lies within the EPR linewidth. Our data described below show that the defect has σ_h symmetry, and hence there are 12 symmetry-related sites. The four sites that arise from differently oriented ⟨111⟩ directions of $\mathbf{A}^{(1)}$ are easily resolved in the EPR, but the further threefold splitting of each of these four spectra is not evident in the EPR spectrum.

Loubser and van Wyk (1985) showed that $\mathbf{A}^{(2)}$ has the opposite sign to $\mathbf{A}^{(1)}$ by observing the onset of motional averaging of the EPR at 600 K.

Newton and Baker (1991a) discussed the various models proposed for N1 and the other common di-nitrogen centres, and produced arguments to suggest that N1

0953-8984/92/418119+12$04.50

Table 1. The ^{14}N hyperfine parameters determined by Shcherbacova *et al* (1969) and Loubser and van Wyk (1985) for the N1 centre. Directions of principal values of hyperfine and quadrupole tensors given as $[\theta, \phi]$, where θ is measured from the [001] crystal axis, and ϕ from the [100] axis while rotating about [001]. Only errors given in the two references quoted.

	Shcherbacova *et al* (1969)	Loubser and van Wyk (1985)
Major nitrogen	$A_{\parallel} = 130(1.5)$ MHz [54.7, 45.0]	$A_{\parallel} = 130.0$ MHz [54.7, 45.0]
	$A_{\perp} = 90(1.5)$ MHz	$A_{\perp} = 90.2$ MHz
Minor nitrogen	$A_{\parallel} = 9.0(9)$ MHz [54.7, 225.0]	$A_{\parallel} = -8.3(1)$ MHz [90.0, 45.0]
	$A_{\perp} = 8.1(9)$ MHz	$A_{\perp} = -7.9(1)$ MHz

corresponds to substitutional nitrogen atoms in second-neighbour sites, as shown in figure 1, one of which has lost an electron. Although this model had been proposed before for another di-nitrogen centre, it had not previously been proposed for N1. Newton and Baker also suggested that this model for N1 should be confirmed by an ENDOR determination of the symmetry of the site and the magnitudes of the quadrupole matrices, which is the motivation for the measurements described in this paper.

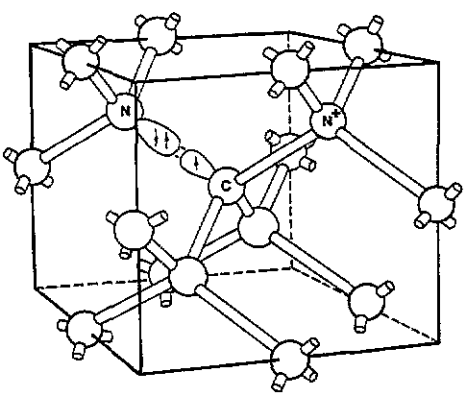

Figure 1. N_1–C–N_2^+ model proposed for N1 defect.

2. Experimental details

2.1. Characterization of the diamond

The diamond, chosen for this study because it showed a strong N1 spectrum, was a natural rounded dodecahedron, with a dark reddish coloration, which is probably due to absorption in the N–V (1.945 eV) band produced by radiation damage.

Parallel faces were polished on the diamond, to allow measurement of the IR absorption spectrum. The defect-induced absorption in the one phonon region was very strong, and saturation could not be avoided. It was not possible to deconvolve the measurements reliably into contributions from the A (Davies 1976), B (Davies 1977) and P1 (Smith *et al* 1959) nitrogen centres, but we estimate the A- and B-centre concentrations to be greater than 500 ppm, and therefore characterize the diamond

as type IaA/B. There was also a very strong narrow peak at 1370 cm^{-1}, associated with a high concentration of platelets (Evans 1973).

Besides the N1 centre, EPR of the diamond used in this study showed that it also contained the O1 (Lomer and Wild 1973), P2 (also known as the N3 optical centre, Davies *et al* 1978), and P1 (Smith *et al* 1959) centres. The presence of O1 clearly showed that the diamond had been electron or neutron irradiated, and annealed to temperatures below 1100 °C, prior to our measurements: we know nothing of previous irradiation treatments.

It was very difficult to estimate the relative concentrations of the EPR defects present because of their different saturation behaviours; however, we note that the P1 concentration was less than that of N1, which was less than that of P2 centres. A typical EPR spectrum, recorded at 4.2 K, is shown in figure 2.

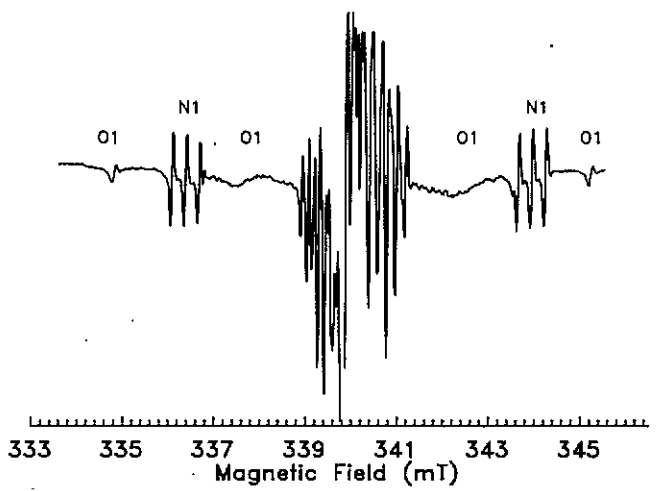

Figure 2. Typical EPR spectrum for diamond containing N1, P2, P1 and O1 centres; recorded at 4.2 K with magnetic field oriented along [001], microwave frequency 9.54 GHz, microwave power $< 10\ \mu W$, field modulation 0.5 G (115 kHz).

2.2. *The TM_{110} ENDOR cavity*

All measurements were made at X-band using a TM_{110} ENDOR cavity constructed in the Clarendon. Several workers (Biehl and Schmalbein 1980, Hurst *et al* 1982, Möhl and de Boer 1985) have made improvements and modifications to the ENDOR cavity described by Biehl *et al* (1975), operating in the TM_{110} mode, with a spiral RF ENDOR coil of same length as the cavity, concentric with the axis. We have found that problems associated with the introduction of the ENDOR coil (i.e. reduction in cavity Q, poor microwave coupling) are entirely overcome by reduction in the length of the RF coil. RF coils were made from 0.7 mm OD copper wire, which was flattened to 0.25 mm, and wound under tension on a 9.0 mm OD former, mounted in a lathe. The pitch of the coil was typically 0.75 turns mm^{-1}, and the length approximately 15 mm. When the tension was released a free standing coil 11.0 mm ID, 11.5 mm OD could be taken off the former. Connections to the ends of the coil were made and passed through the side wall of the cavity, and soldered to terminals. Standard

BNC connectors make a press-fit contact with these terminals. The connections to the coil are perpendicular to, and in the nodal plane of the microwave E-field of the chosen mode. Introduction of the coil shifted the frequency by 100 MHz, and did not degrade the Q of the resonator noticeably. The unloaded Q of the microwave cavity was approximately 4000. A schematic diagram of the cavity is shown in figure 3.

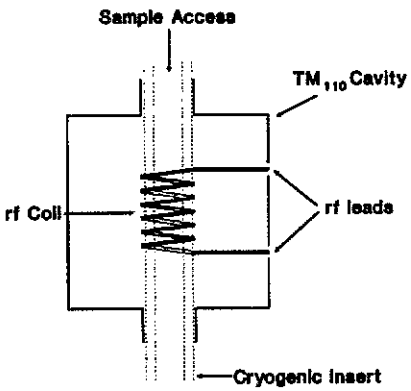

Figure 3. TM_{110} ENDOR cavity, showing position of the ENDOR coil.

The field modulation coil was wound in the nodal E-field plane of the selected microwave mode, as close to the centre of the cavity as possible. Not only did this provide an efficient field modulation, but also it suppressed unwanted modes, in the same way as the modification described by Biehl and Schmalbein (1980). In all other respects the ENDOR cavity was conventional, constructed in silver-plated brass, radius 17.25 mm, length 30 mm, resonant frequency 9.75 GHz with 11.0 mm Oxford Instruments quartz insert (10.57 GHz without insert). Microwave coupling was accomplished with an iris/coupling screw mechanism on the side of the cavity.

The reduction in length of the RF coil should not dramatically reduce the RF field generated at its centre. From simple geometrical considerations, reducing the length from 30 to 15 mm, for a coil of radius 5.5 mm, should reduce the RF magnetic field at the centre of the coil by only 15%. The RF field was measured by the method of Hyde (1965); we estimate that at 25 MHz, an RF field of approximately 0.5–0.8 mT (in the rotating frame) can be generated with 100 W of RF power (coil 15 mm long, radius 5.5 mm, 0.75 turns mm^{-1}).

3. Results

3.1. ENDOR measurements

CW ENDOR measurements were made on both nitrogen atoms of the N1 defect at nominally 5 K, using the technique described by Newton and Baker (1991b). In this experiment one RF frequency is swept rapidly and repeatedly through the nuclear transitions, resulting in a large enhancement of the EPR, while a second is swept slowly, so stimulating ENDOR which is detected in a conventional manner at higher signal-to-noise ratio. This enhanced the CW ENDOR signal-to-noise ratio by up to an order of magnitude over that of conventional ENDOR. ^{14}N ENDOR transitions were detected in the range 1 to 70 MHz with very good signal-to-noise ratio. Accurate

ENDOR measurements were made on EPR transitions belonging to different symmetry-related sites with the external magnetic field carefully aligned along ⟨100⟩, ⟨110⟩, and ⟨111⟩ directions. The anisotropic nature of the ENDOR spectra and the narrow linewidth (60 kHz) made very precise orientation possible (±0.05°). An isotropic ENDOR resonance, detected at 3.65 MHz was attributed to natural-abundance ^{13}C (distant ENDOR).

The transmission line supplying the RF power for ENDOR was either terminated with the RF coil itself, or interrupted by the coil and terminated with a 50 Ω load. We find that driving directly into the coil is particularly useful when looking at low-frequency (1–5 MHz) resonances, as maximizing the current in the coil, and hence the RF magnetic field, is essential to drive these nuclear transitions towards saturation. The effects of different RF loads is shown in figure 4 for low-frequency ^{14}N and ^{13}C ENDOR from the N1 centre.

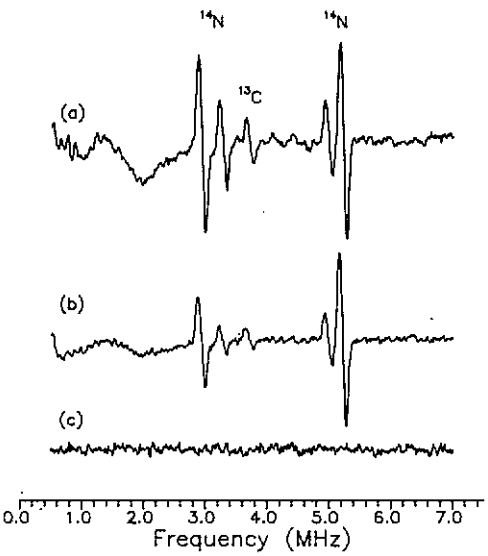

Figure 4. ^{14}N and ^{13}C ENDOR from the N1 di-nitrogen centre in diamond. Microwave frequency 9.547 GHz, temperature 6.0 K, field modulation (115 KHz) 0.25 G, RF frequency modulation (FM) 87 Hz, FM depth 60 kHz, RF amplifier ENI 420L (20 W) output maximum (300 mV input), (a) RF line terminated with ENDOR coil, (b) RF line terminated with 50 Ω load, and (c) same conditions as (a) but for magnetic field off EPR resonance.

3.2. Fitting the spin-Hamiltonian parameters

We fitted the Hamiltonian given in equation (1) to the experimental data in two ways: (a) while constraining the major and minor nitrogen hyperfine and quadrupole interactions to {110} symmetry (7 varied parameters); and (b) while letting them vary arbitrarily (11 varied parameters), in order to determine if there was a true {110} plane of symmetry. The χ^2-fit used the best estimate for the individual standard deviations in the data points. Though the χ^2 was slightly larger for the constrained fit (a), the computed probabilities (assuming that the measurement errors are approximately normally distributed) estimating the 'quality of fit', are about the same for both approaches. It appears that constraining the N1 defect to σ_h symmetry is reasonable, and from our data we must deem the models acceptable on equal terms, i.e. any distortion lowering the σ_h symmetry is not significant. The experimental RMS standard deviation from the best χ^2-fit was slightly larger for the ENDOR lines from the major nitrogen (0.005 MHz) than for the minor nitrogen (0.003 MHz). The reasons for this included greater sensitivity to misorientation, lower signal-to-noise ratio, and

Table 2. Principal values of the ^{14}N hyperfine and quadrupole parameters for both nitrogens of the N1 centre determined in the present study. Directions of principal values of hyperfine and quadrupole tensors given as $[\theta, \phi]$, where θ is measured from the [001] crystal axis, and ϕ from the [100] axis while rotating about [001]. Errors given in brackets.

Nitrogen N_1		Nitrogen N_2	
$\mathbf{A}^{(1)}$ (MHz)	$\mathbf{P}^{(1)}$ (MHz)	$\mathbf{A}^{(2)}$ (MHz)	$\mathbf{P}^{(2)}$ (MHz)
89.218(4)	+1.213(1)	−8.327(2)	+0.0437(6)
[90°, 135°]	[90°, 135°]	[90°, 135°]	[90°, 135°]
126.355(4)	−2.388(1)	−7.875(2)	−0.2077(6)
[55.15(5)°, 45°]	[54.79(5)°, 45°]	[70.2(1)°, 225°]	[72.18(5)°, 225°]
89.198(4)	+1.175(1)	−8.288(2)	+0.1639(6)
[34.84(5)°, 225°]	[35.21(5)°, 225°]	[19.8(1)°, 45°]	[17.82(5)°, 45°]

overlap of different resonances. The fitted hyperfine and quadrupole parameters for both nitrogen atoms of the centre are given in table 2.

Gross misorientation caused a splitting in the ENDOR lines, but small misorientations only modified the ratios in intensities between different lines in the spectra. Our simulations show that for orientation errors smaller than 0.05° no effect can be observed in the ENDOR spectra. To make a realistic estimate of the errors in the magnitude and principal directions of hyperfine and quadrupole parameters, the input data sets were modified with a gaussian-weighted error on all the transition frequencies, and the χ^2-fit repeated. The uncertainties determined are given in table 2.

The hyperfine and quadrupole matrices for the major nitrogen are close to axial symmetry. In this approximation, the parameters are compared in table 3 with those for other centres in diamond. The hyperfine parameters have been factorized into an isotropic part $A_s = [\frac{1}{3}(A_\parallel + 2A_\perp)]$ and a traceless part $A_p = [\frac{1}{3}(A_\parallel - A_\perp)]$. The unpaired electron orbital on the nitrogen is assumed to be $\psi = \eta(\alpha\psi_{2s} + \beta\psi_{2p})$, where α, β, η are deduced from the hyperfine parameters in the usual way (e.g. Watkins and Corbett 1961, Morton and Preston 1978). The fraction of unpaired electron in the 2p orbital on the nitrogen is $f_{2p} = \eta^2\beta^2$, and the hybridization ratio $\lambda^2 = \beta^2/\alpha^2$.

Table 3. $^{14}N_1$ hyperfine constants A_s and A_p, η^2, λ^2 and f_{2p} (computed using experimental values of A_s and A_p, and those calculated for 100% occupancy of 2s and 2p orbitals on the free atom, Morton and Preston 1978) and quadrupole parameters.

	A_s (MHz)	A_p (MHz)	η^2	λ^2	f_{2p}	$P_\parallel$ (MHz)
N4‡	74.2(3)	8.6(3)	0.196	3.78	0.155	?
P1†	92.228(1)	10.903(2)	0.247	3.85	0.196	−3.974(1)
W7‡	97.79(3)	11.79(3)	0.267	3.93	0.213	−3.82(4)
N1	101.590(5)	12.38(1)	0.279	3.97	0.223	−3.582(1)

‡ Newton and Baker (1991a).
† Cook and Whiffen (1965).

The hyperfine parameters in table 2 are seen to lie within the probable uncertainty of those given in table 1 for EPR, but to differ in the following details (specified for one of the centres for which (110) is the σ_h plane).

(i) The hyperfine matrix for N1 has approximate axial symmetry, like that for P1, but the principal axis is tipped by 0.4° from [111], and its magnitude indicates a 13% larger density of unpaired electron on N_1, with a 3% increase in λ^2. The quadrupole interaction matrix for N_1 is hardly significantly distorted from having [111] as a principal axis, though there is small departure from axial symmetry, and its magnitude is 10% smaller than for P1.

(ii) The hyperfine matrix $\mathbf{A}^{(2)}$ for N_2 is negative, $A_s = -8.16$ MHz, and the anisotropic component is very small. The symmetry is not quite axial, but it approximates to it with $A_p = +0.144$ MHz about a direction tipped 15.5° from $[\bar{1}\bar{1}1]$ towards $[\bar{1}\bar{1}0]$. Very approximately, the quadrupole interaction has the form $P_{xx} = -P_{zz}$, with $P_{yy} = 0$ normal to the (110) plane; the z-direction making an angle tipped 17.4° from $[\bar{1}\bar{1}1]$ towards $[\bar{1}\bar{1}0]$.

4. Discussion

4.1. The model of the N1 centre

Models that have been previously proposed by various authors for N1 have been discussed by Newton and Baker (1991b) in sections 3 and 4, so we will not repeat that detail here.

The principal properties of N1 which have to be accounted for by a model are as follows.

(i) Our ENDOR measurements show that the site symmetry is σ_h, and that the parameters for the major nitrogen (N_1) are similar to those for P1, and those for the minor nitrogen (N_2) show that it is almost tetrahedral N^+. Hence, the centre must comprise a P1 centre which is slightly perturbed by a second N^+ atom in the {110} plane which contains P1.

(ii) The motional averaging of the EPR at high temperatures shows that the two nitrogen atoms can exchange roles by tunnelling of the unpaired electron between them, so they must occupy symmetrically related sites in the centre. It shows further that the ⟨111⟩ directions of the principal directions of the P1 sites for these nitrogens are different. The activation energy for this hopping (0.4 eV, Loubser and van Wyk 1985) is smaller than that for the hopping process in P1 centres (0.76 eV, Loubser and van Ryneveld 1967).

Starting with P1 (N_1–C) as a basic component of the defect, we have to determine where the N_2^+ lies in the {110} plane, and whether there are other perturbing features in the same plane. Figure 5 shows the P1 centre, and the other carbon atom sites in the relevant {110} plane. N_2^+ cannot lie at an interstitial site, as when the two nitrogen atoms exchanged roles by the transfer of the unpaired electron, an entirely different centre would be formed. The even-numbered sites in figure 5 are ruled out as possible sites for N_2, because when N_1 and N_2 exchanged roles, the two sites would be related by inversion, which would not change the principal axis of the P1 component, contrary to the observation mentioned in (ii) above.

Some of the odd-numbered sites are ruled out by the magnitude of A_s in comparison with ^{13}C hyperfine parameters of similarly placed C atoms in the P1 centre (Barklie and Guven 1981): for an equivalent electronic wavefunction on ^{14}N, the value of A_s would be halved. For ^{13}C, A_s exceeds 12 MHz only for sites 4, 7 and

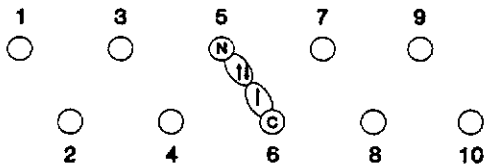

Figure 5. Carbon atoms surrounding single substitutional nitrogen (P1) defect, in a chosen {110} plane. For details of labelling see text.

8, and no other site has A_s larger than 8.2 MHz. Hence, the measured A_s for N_2 is too large for sites 3 or 9. This leaves only site 7, as suggested for this centre by Newton and Baker (1991b).

We should also consider whether a vacancy or substitutional impurity could be involved in the centre. The requirement for symmetry relative to N_1 and N_2, makes site 6 the only possible place for a vacancy or impurity. The lack of observed ^{13}C hyperfine structure from the unique carbon at site 6 is suggestive that the atom may be missing or replaced by an element with low abundance of isotopes with nuclear moments. However, the non-observance may simply be due to its small signal strength and the uncertainty in its magnitude. It would be very interesting to measure its **A** matrix, as unlike for P1 it would not be axially symmetrical. A vacancy (V) at site 6 would destroy the P1 component by removing its principal C atom. Also, the centre $(N_1\text{–}V\text{–}N_2)^+$ would have C_{2v} symmetry with the unpaired electron presumably in a N_1–N_2 anti-bonding orbital, making the two nitrogen atoms equivalent. Furthermore, the centre formed by two N atoms adjacent to a vacancy is already known as the H3 centre (2.463 eV absorption band): it is not paramagnetic, and is a commonly observed optical centre in diamond, formed when a vacancy is trapped by an A centre (Davies 1977). An impurity at site 6 would also destroy the P1 component, unless it were good at mimicking C, like Si or Ge, or even B^-, but such substituted elements would give readily observable hyperfine interactions with their odd nuclei, which are not observed.

It therefore seems that alternatives to the $N_1\text{–}C\text{–}N_2^+$ model do not fit the observed properties. It is of interest to see how far we can account for the details of the observed properties with this model.

4.2. Details of the hyperfine interactions

From table 3, we see that f_{2p} increases and $|P_{\|}|$ decreases through the series P1 → W7 → N1. Messmer and Watkins (1972) predict such behaviour as the N_1–C bond length decreases. (We have no reason to believe that calculations of f_{2p} and $P_{\|}$ based upon the more recent calculations (Briddon *et al* 1991, Kajihara *et al* 1991) would not show the same behaviour.) Further, the larger $\mathbf{A}^{(1)}$ and λ^2 in N1 compared with P1 indicates a shorter N_1–C bond, but with a greater displacement of the nitrogen, suggesting a smaller displacement of the unique carbon. This could account for the lower activation energy for motional averaging.

Newton and Baker (1991b), section 4, have accounted for the small negative value of $A_s^{(2)}$ as resulting from partial cancellation between a negative indirect contribution from spin polarization and a positive direct contribution. Even more remarkable is that $A_p^{(2)}$ is much smaller than the dipolar interaction ($A_d^{(2)}$) between the unpaired

electron in the N_1–C bond and the $^{14}N_2$ nucleus. If $\Psi(r)$ represents the wavefunction of the unpaired electron, primarily located on the unique carbon atom and N_1, the dipolar interaction between this electron and the ^{14}N nucleus of N_2 at $\boldsymbol{R}$ is given by

$$\boldsymbol{S}\cdot\mathbf{A}_{\mathrm{d}}^{(2)}\cdot\boldsymbol{I} = \frac{\mu_0}{4\pi}\mu_{\mathrm{B}}\mu_{\mathrm{N}}g g_{\mathrm{N}}\int \Psi^*(r)\Psi(r)\left(\frac{\boldsymbol{S}\cdot\boldsymbol{I}}{r^3} - \frac{3(\boldsymbol{S}\cdot(\boldsymbol{R}-r))(\boldsymbol{I}\cdot(\boldsymbol{R}-r))}{r^5}\right)\mathrm{d}^3r. \tag{2}$$

The integral may be approximated by taking 28% of the magnetic moment of the unpaired electron to be centred on the N_1 nucleus and 72% on the unique carbon nucleus. This gives $A_{\mathrm{d}} = 1.15$ MHz in principal direction $[\theta,\phi] = [57.3°, 225°]$. If, as for transferred hyperfine interaction with ligand ions, e.g. in CaF_2, the anisotropic component of $\mathbf{A}^{(2)}$ is written as $\mathbf{A}_{\mathrm{d}}^{(2)} + \mathbf{A}_{\mathrm{p}}^{(2)}$, subtraction of the calculated $\mathbf{A}_{\mathrm{d}}^{(2)}$ leads to an approximately axially symmetrical $\mathbf{A}_{\mathrm{p}}^{(2)}$, with $A_{\mathrm{p}}^{(2)} \simeq -1.0$ MHz, and the principal direction, $[\theta,\phi] = [55.6°, 225°]$, being tipped only 0.9° from $\langle\bar{1}\bar{1}1\rangle$ (N_1–C is almost along $\langle 111\rangle$). $A_{\mathrm{p}}^{(2)}$ has the same sign as $A_{\mathrm{s}}^{(2)}$ and suggests a p:s ratio (λ^2) of 4.4 which is reasonable. This analysis can be regarded only as very approximate, as we are making no explicit calculation of the indirect spin polarization, but it is indicative that the model can account for the measured interaction.

4.3. Details of the quadrupole matrix for the major nitrogen

The fine details of the quadrupole matrices are more difficult to account for. Unlike the **A** matrices, which depend only upon the distribution of the unpaired electron, the **P** matrices depend upon the distribution of all of the 2p electrons on the N atoms, as they give rise to the main part of the electric field gradient at the ^{14}N nuclei. Analysis of the details of $\mathbf{P}^{(1)}$ suggests that the contribution from N_2^+ to the electric field gradient at N_1 is not large, and that the small distortion from axial symmetry must result from a small change in bond angles.

4.4. Details of the quadrupole matrix for the minor nitrogen

The characteristic feature of $\mathbf{P}^{(2)}$ is its approximation to $P_{yy} = 0$, so that $P_{zz} = -P_{xx}$. It is also, as predicted by Baker and Newton (1991b), larger in magnitude than that found for the minor nitrogen in the W7 centre, because the minor nitrogen is closer to the extra electron in the N_1–C bond. The proximity to N_1–C is expected to increase the distortion of the atomic positions, and create larger imbalances in the charge distribution around N_2^+. The small $\mathbf{P}^{(2)}$ indicates very little distortion from tetrahedral symmetry, and therefore that the displacement of the unique carbon of the N_1–C–N_2^+ structure is smaller than that of the P1 centre (14% of the C–C bond, Kajihara *et al* 1991, Briddon *et al* 1991). This is consistent with the preceding discussion on the hyperfine and quadrupole interactions of N_1.

We can calculate expressions for the elements of $\mathbf{P}^{(2)}$ in terms of the three angles θ_1, θ_2, and $\theta_3 = \theta_4$ (shown in figure 6) by making the assumptions that (a) the electric field gradient is due to the electrons occupying the 2p orbitals surrounding the nitrogen nucleus; (b) the distortion from tetrahedral coordination is very small, so the changes in p:s ratio of the nitrogen orbitals can be ignored; this is equivalent to saying that the orbitals remain sp^3 but are tilted a little from the $\langle 111\rangle$ directions; (c) the occupation of the four orbitals around the nitrogen is identical; (d) the local environment of the nitrogen is constrained to have a $\{110\}$ symmetry plane.

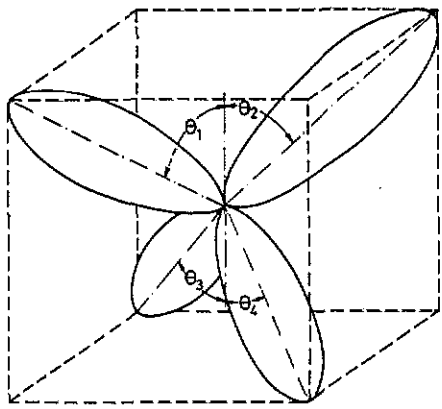

Figure 6. Schematic diagram of the sp^3 orbital around the N^+. Each orbital makes an angle θ_n with the vertical. The orbital labelled with the angle θ_1 is directed towards the unique carbon of the defect.

Using a factor $P_0 = -4.3$ MHz for the principal value of the quadrupole interaction that would result from a single electron in a single sp^3 hybrid (Edmonds *et al* 1972), we calculate that an interaction matrix consistent with that measured is produced for $\theta_1 = 54.85°$, $\theta_2 = 55.99°$, and $\theta_3 = \theta_4 = 54.57°$ ($\theta = 54.74$ for an undistorted site). The result is encouraging, as we have shown that the observed quadrupole interaction can be produced by only a very small distortion, and may confirm the suggestion made above that the displacement of the unique carbon is much less in N1 than P1.

Hence, we have shown that the N_1–C–N_2^+ model is in qualitative agreement with all measured properties, and that no other atomic model can account for them.

5. Formation of the N1 centre

Now that the N1 centre is characterized, it is of interest to speculate how it is formed and why it appears in the diamond we have investigated. We also wish to examine further a question which was discussed briefly by Newton and Baker (1991b); that of why the N_1–C–N_2 centre is ionized. Even in diamond containing as much as 1000 ppm single substitutional nitrogen the probability of statistical occurrence of any particular di-nitrogen centre is only about 1 ppm, and all possible neighbouring sites for N_2, relative to a specific N_1, would be occupied with equal probability. Hence the di-nitrogen centres, which have been observed, occur in far more than statistical probability.

The aggregation of nitrogen has been studied by several workers (Chrenko *et al* 1977, Evans and Qi 1982, Collins 1980). Under appropriate conditions of temperature and stabilizing pressure, single substitutional nitrogen atoms aggregate to form A centres (N–N diamagnetic nearest-neighbour pairs). More severe conditions allow aggregation of A centres to form B centres (Evans and Qi 1982). It seems that nitrogen atoms can diffuse by N↔C interchange, as well as by a vacancy-mediated mechanism proposed by Collins (1980).

During aggregation of P1 to A centres (without involving vacancies in the final step), the nitrogen atoms must pass through the second-neighbour position, N–C–N. Interchange of N and C leads to the A centre which is stable presumably because the energy of the full N–N antibonding orbital containing two electrons lies lower in the band gap than that of P1. We speculate that the stable configuration of N–C–N could be $N–C^{-}–N^{+}$, where the P1 centres have cooperated to form a full $N–C^{-}$ antibonding orbital, adjacent to a relatively strain-free N^{+}. Ionization of $N–C^{-}–N^{+}$ would lead to the formation of the N1 centre, which, as we observe it, we presume to be stable to further evolution. Even if $N–N^{+}–C$ were formed, it would probably be a very efficient electron trap, converting itself to the A centre. Therefore the only requirement of formation of N1 beyond normal aggregation is the presence of a suitable electron trap. This mechanism accounts for the concentration of N1 being much larger than one would expect for a random distribution of nitrogen: without ionization the $N–C^{-}–N^{+}$ unit would either break up or an A centre would result.

6. Conclusion

The new ENDOR measurements on the N1 centre confirm the $N_1–C–N_2^{+}$ model for the defect. The N^{+} is in a substitutional site with approximately tetrahedral symmetry. The $N_1–C$ fragment of the centre resembles the P1 centre, with slightly larger unpaired electron density on the nitrogen, and a smaller quadrupole interaction. This information is consistent with a smaller unique $N_1–C$ bond extension in the N1 centre than that of the P1 centre. This, taken with the **A** and **P** matrices for the N^{+}, implies that the unique carbon undergoes a much smaller displacement from the tetrahedral lattice site than in the case of P1. Further work is required if we are to understand the formation process of the N1 centre.

Acknowledgments

Dr R J Caveney and his associates at the Diamond Research Laboratory, De Beers Industrial Diamond Division, Johannesburg, for providing samples and their continued interest in the research programme. Dr J A van Wyk and Professor J H N Loubser of the University of the Witwatersrand, for many helpful discussions. AC and MEN thank the Science and Engineering Research Council for a maintenance grant, and a Postdoctoral Research Fellowship, respectively. We thank Professor J A Weil, Dr D G McGavin and Dr M J Momborquette for the simulation and fitting software EPR.FOR.

References

Ammerlaan C A J 1990 *Landolt–Börnstein Numerical Data and Functional Relationships in Science and Technology* New Series III, vol 22b, ed O Madelung and M Schulz (Berlin: Springer) pp 117–206

Barklie R C and Guven J 1981 *J. Phys. C: Solid State Phys.* **14** 3621

Biehl R, Plato M and Mobius K 1975 *J. Chem. Phys.* **63** 3515–22

Biehl R and Schmalbein D 1980 *US Patent Appl. No* 142652

Briddon P R, Heggie M I and Jones R 1991 *Proc. 2nd Int. Conf. on New Diamond Science and Technology* ed R Messier, T J Glass, J E Butler and R Roy (Pittsburg, PA: Materials Research Society) p 63

Chrenko R M, Tuft R E and Strong H M 1977 *Nature* **270** 141
Colins A T 1980 *J. Phys. C: Solid State Phys.* **13** 2641
Cook R J and Whiffen G H 1966 *Proc. R. Soc.* A **295** 99
Davies G 1976 *J. Phys. C: Solid State Phys.* **9** L537
—— 1977 *Chem. Phys. Carbon* **13** 1
Davies G, Welbourn C M and Loubser J H N 1978 *Diamond Research* (supplement to the *International Diamond Review*) (Ascot: De Beers Industrial Diamond Division) p 23
Edmonds D T, Hunt M J and Mackay A L 1972 *J. Magn. Reson.* **9** 66
Evans T 1973 *Diamond Research* (supplement to the *International Diamond Review*) (Ascot: De Beers Industrial Diamond Division) p 2
Evans T and Qi Z 1982 *Proc. R. Soc.* A **381** 159
Farrer R G 1969 *Solid State Commun.* **7** 685
Hurst G, Kraft K, Schultz R and Kreilick R 1982 *J. Magn. Reson.* **49** 159–60
Hyde J S 1965 *J. Chem. Phys.* **43** 1806
Kajihara S A, Antonelli A, Bernholc J and Car R 1991 *Phys. Rev. Lett.* **66** 2010
Lomer J N and Wild A M A 1973 *Radiat. Eff.* **17** 37
Loubser J H N and Ryneveld W P 1967 *Br. J. Appl. Phys.* **18** 1029
Loubser J H N and van Wyk J A 1978 *Rep. Prog. Phys.* **41** 1201
—— 1985 *Mater. Res. Soc. Symp. Proc.* **46** 587
Messmer R P and Watkins G D 1973 *Phys. Rev.* B **7** 2568
Möhl W and de Boer E 1985 *J. Phys. E: Sci. Instrum.* **18** 281
Morton J R and Preston K F 1978 *J. Magn. Reson.* **30** 577
Newton M E and Baker J M 1991a *J. Phys.: Condens. Matter* **3** 3605
—— 1991b *J. Phys.: Condens. Matter* **3** 3591
Shcherbacova M Ya, Sobolev E V, Samsonenko N D and Aksenov V K 1969 *Sov. Phys.–Solid State* **11** 1104
Smith W V, Sorokin P P, Gelles I L and Lasher G J 1959 *Phys. Rev.* **115** 1546
Watkins G D and Corbett J W 1961 *Phys. Rev.* **121** 1001